Available online at www.sciencedirect.com

ScienceDirect

Procedia Structural Integrity 23 (2019) 95–100

Structural Integrity Procedia

www.elsevier.com/locate/procedia

9th International Conference on Materials Structure and Micromechanics of Fracture

Neutron investigation of Nitinol stents and massive samples before and after PIRAC coating

M. Rogante[a]*, J. Buhagiar[b], G. Cassar[b], M. Debono[b], V. Lebedev[c], P. Mikula[d], V. Ryukhtin[d]

[a]*Rogante Engineering Office, Contrada San Michele, n. 61, 62012 Civitanova Marche, Italy*
[b] *Department of Metallurgy & Materials Engineering, Faculty of Engineering, University of Malta, Msida MSD 2080, Malta*
[c]*Petersburg Nuclear Physics Institute, Gatchina, St. Petersburg, Russian Federation*
[d]*Nuclear Physics Institute ASCR and Research Centre Řež, Ltd., 25068 Řež, Czech Republic*

Abstract

Nitinol, a thermoelastic Ni-Ti Shape Memory Alloy (SMA) with approximately 50 at. % Ti, is adopted in a wide range of medical equipment and devices used in interventional radiology, orthopaedics, neurology and cardiology, in particular as a smart material for stents. In this work, NiTi real stents and massive samples before and after different Powder Immersion Reaction Assisted Coating (PIRAC) treatments have been investigated by using two neutron techniques: (1) Small and Ultra-Small Angle Neutron Scattering (SANS, USANS) for nano- and micro-scale characterization, obtaining information on structure and the effects due to the coating treatment; and (2) High-Resolution Neutron Diffraction (HRND), evaluating the macrostrain components resulting from angular shifts of diffraction peaks and the micro-strains in the plastically deformation region by means of profile-broadening analysis. The obtained results contribute: improving knowledge of defects and other key features of the materials complementary to those achieved by using traditional examination techniques; helping to better understand the functional characteristics of Nitinol parts and predict the material's mechanical behaviour.

Keywords: Nitinol; Shape memory alloys; SANS; USANS; High-Resolution Neutron Diffraction; nanostructure.

* Corresponding author. Tel.: +390733775248; fax: +390733775248.
E-mail address: main@roganteengineering.it

10.1016/j.prostr.2020.01.069

1. Introduction

Nitinol, a thermoelastic NiTi shape memory alloy with approximately 50 at. % Ti, is adopted in a wide range of medical equipment and devices used in interventional radiology, orthopedics, neurology and cardiology, in particular as a smart material for stents. Fracture occurrences of up to 50%, probably due to in vivo cyclic displacements, have been reported in a number of Nitinol stents after one year. Knowledge of nanostructure of this material, thus, is fundamental to understand the damage micro-mechanisms, especially with reference to the consequences of the geometrically reversible stress-induced martensitic phase transformation on crack-growth resistance; Rogante et al. (2011a); Rogante et al. (2011b).

A novel surface engineering technique called Powder Immersion Reaction Assisted Coating (PIRAC) can produce well-adherent, uniform TiN coatings on NiTi products. It is a simple diffusional process which is based on the immersion of samples into powders of an unstable nitride (such as Cr_2N), and their subsequent annealing at high temperatures in chromium-rich stainless steel foil bags; Zorn et al. (2008) and Starosvetsky & Gotman (2001). No work has been made to characterize PIRAC using Neutron characterization techniques.

In the present work, Small Angle Neutron Scattering (SANS), Ultra-Small Angle Neutron Scattering (USANS) and High-Resolution Neutron Diffraction (HRND) have been adopted.

Nomenclature

A	parameter related to the scattered intensity
D	slope of scattering function
I_0	zero angle scattering intensity, arb. un.
$P(R)$	distributions of the distances
Q	momentum transfer, $Å^{-1}$
R	pores size, nm
R_c	correlation radius, nm
R_g	gyration radius, nm
r_g	gyration radius of the system of defects, nm
$\Delta\omega$	rocking angle

2. Materials and samples

NiTi coupons (Brindley Metals Ltd, UK) of 25.4 mm in diameter were polished to a mirror finish and ultrasonically cleaned in isopropyl alcohol. The samples were subjected to a treatment called Powder Immersion Reaction Assisted Coating (PIRAC) at 900ºC for 1.5 hours and 3 hours followed by a water quench. Treatment details can be found in the paper by Starosvetsky & Gotman (2001). However, a number of modifications were introduced in the treatment presented in this work. The prepared PIRAC bags were each inserted into similar bags of a larger size for additional protection from atmospheric oxygen. Additionally, Zr pellets (getter) were also added in both the inner and outer bags to act as an oxygen scavenger. The getter had a surface area of 45 cm^2 and of 60 cm^2 in the inner and outer bags respectively.

The analyzed NiTi samples of Fig. 1 were: A) massive, untreated; B) massive, submitted to PIRAC at 900°C for 1.5h and water quenched - coating thickness: TiN (0.1 μm) + Ti2Ni (0.6 μm); C) massive, submitted to PIRAC at 900°C for 3h and water quenched - coating thickness: TiN (0.5 μm) + Ti2Ni (0.6 μm); D, E) commercial stents.

Samples A, B and C have been produced by the Department of Metallurgy & Materials Engineering of the University of Malta. Samples D and E have been supplied by the Neuroradiology Dept., Azienda USL, Emilia-Romagna Region Health Service, Italy.

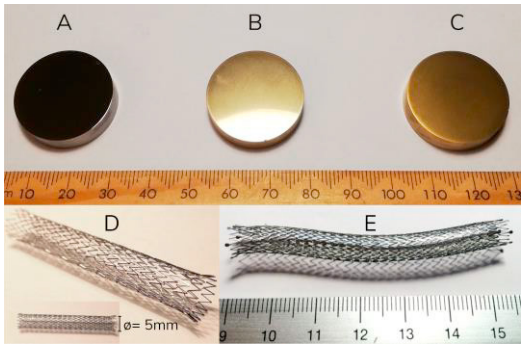

Fig. 1. The analyzed Nitinol samples.

3. Measurements, results and discussions

The massive Nitinol samples A, B and C have been initially tested by the double-bent crystals SANS instrument MAUD of CANAM-NPI, Řež, Czech Republic; Strunz et al. (1997). Measurements were carried out at ambient temperature in a wide range of momentum transfer Q = 0.0002÷0.02 Å^{-1}. The aim of experiment was to determine the structural features of various defects in the considered massive samples as dependent on thermal treatment. Such defects can be precipitates, voids, dislocation groups and borders of crystallites. The measured SANS scattering curves are shown in Fig. 2.

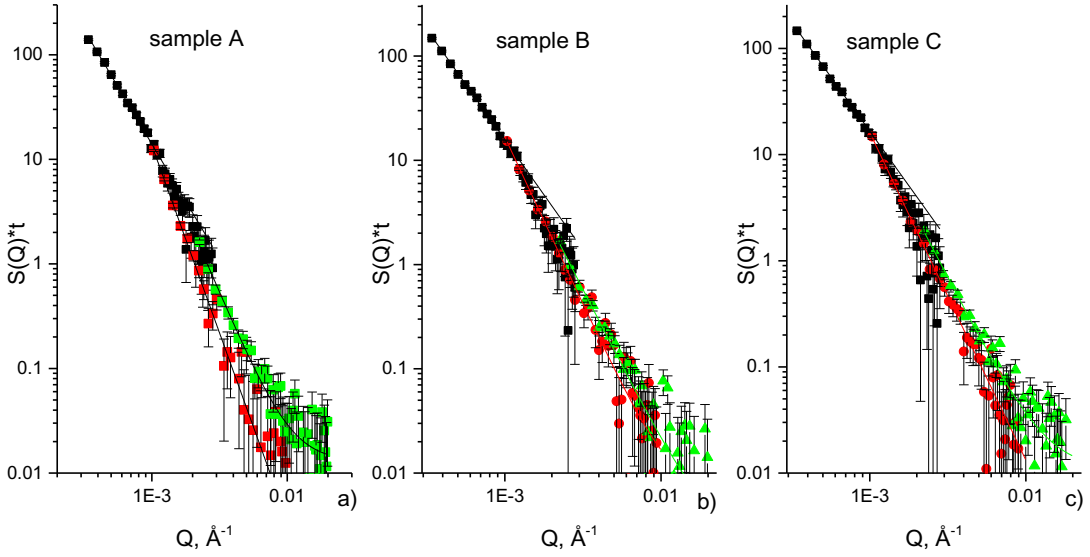

Fig. 2. Scattering intensity *I(q)* vs. momentum transfer for the massive Nitinol samples A, B and C (1-3). The lines show the fitted functions for different instrumental resolutions.

The data were measured using 3 different resolutions – high, medium and low. These parts of SANS data were fitted using power law functions including incoherent background $A*Q^D+bkg$. The power parameter D represents the structural features, graphically in log-log scale D it corresponds to the slope of the scattering function. The fitted D parameters are summarized in Fig. 3.

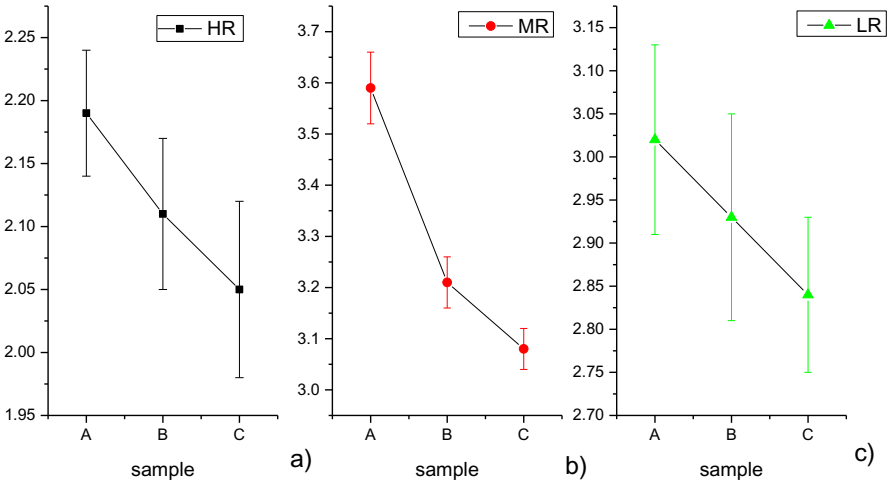

Fig. 3. Fitted power law parameters D for high (a), medium (b) and low resolution parts.

SANS data can be divided into 2 parts, i.e. the low Q (Q<0.001 Å^{-1}) and the high Q region (Q>0.001 Å^{-1}) according to power law behavior. In the low Q region the slope parameter D is close to -2 (Fig. 3a), which might be caused to the scattering by 2D objects (e.g. disk-like particles). SANS curves in the high Q region demonstrate the classical Porod law for infinite slit geometry experiment, since with power exponent $D \sim -3$ (Fig. 3c). In the medium resolution data (Fig. 3b), mostly laying in the high Q region, a clear decreasing trend appears of D towards the Porod value of -3 with increasing of annealing time. This means that mean sized inhomogeneities (most probably, pores of size $R \sim 100 \div 500$ nm) are disappearing. Larger scattering objects (R > 500 nm), nevertheless, are still present, despite they can't be fully characterized because the Guinier region is limited by the instrumental resolution. The fitted parameter A, which is related to the scattering intensity at $Q \rightarrow 0$, nevertheless, shows slightly increasing with aging time (Fig. 4). This means that the small pores or other scattering objects coalesced to larger ones since the zero angle scattering I_0 is proportional to volume fraction; Feigin & Svergun (1987).

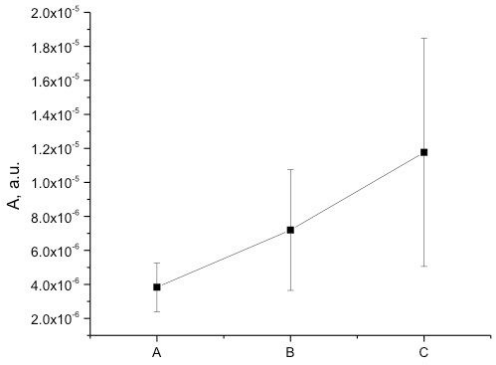

Fig. 4. Fitted parameter A for high resolution SANS data.

Samples A, B and C were also tested at 18°C by adopting the high resolution three axis neutron optic diffractometer of the CANAM; Mikula et al. (2019). The obtained rocking curve (i.e., intensity vs. rocking angle $\Delta\omega$ near the Bragg angle qA) related to the sample B is reported in Fig. 5.

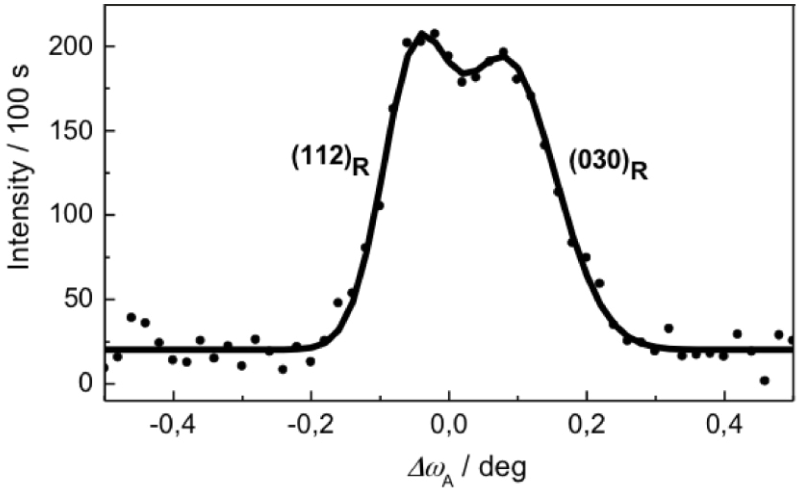

Fig. 5. Diffraction profile obtained for sample B as analysed by BPC Si(311) analyser. The curves are fitted by two Gaussians.

As a result, the PIRAC temperature has shown an influence on the Nitinol quality, and that two close reflections of the *R*-phase could be visibly identified, specifically, for the PIRAC at 900 °C for 1.5 hour (sample B).

The commercial Nitinol stent samples D and E, instead, were tested by the YS-SANS instrumentation of BNC, Budapest. The SANS q-dependence is shown in Fig. 6a. The curve *I(q)* has been used to obtain the distributions of the distances *P(R)* (Fig. 6b) between the scattering centres (defects in material), which ensemble gives the resulting data of Fig. 6a. This treatment has provided the determination of the effective gyration radius of the system of defects, r_g = 11.7 ±0.02 nm, and the forward intensity $I(q \rightarrow 0)$ = (0.003914 ±0.0000024) arb. un.

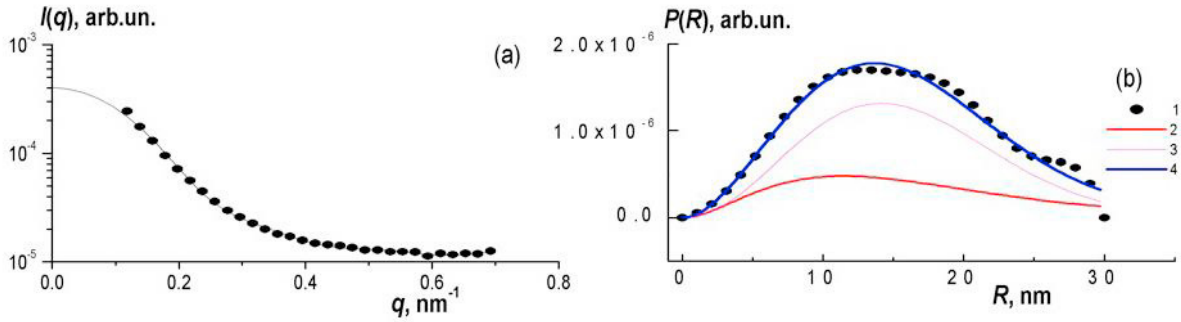

Fig. 6. SANS-intensity (a) and distribution function *P(R)* (b). The scattering function (a) is presented (line) and the related data P(R) (b, data 1), the partial (2,3) and total (4) correlation functions are shown.

A more detailed analysis of the correlation function $\gamma(R) = P(R)/R^2$ (Fig. 7) has shown two characteristic scales ($R_C < R_L$) for the observed correlations and the data obey the model function:

$$\gamma(R) = g_1 exp(-R/R_C) + g_2 exp[-(R/R_L)^2] \quad (1)$$

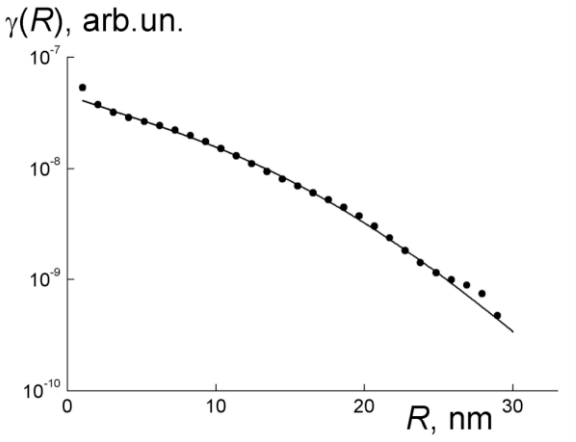

Fig. 7. Correlation function vs. radius. The line is the fitting function (eq. 1).

The first term of eq. 1 is a contribution from the globular particles (e.g., nano-phase inclusions) having the correlation radius R_C = 5.7±0.9 nm. The second term represents some assembly of these entities into more extended structures with a correlation radius R_L = 14.1 ± 0.5 nm. The issued gyration radius of such a structure is equal to $R_g=R_L(3/4)^{1/2}\approx$12.2 nm that is approximately the averaged radius above obtained, $r_g\approx$12 nm. The structure of the considered Nitinol stents at the scales R ~ 1 – 30 nm, thus, can be considered as composed of tiny particles (size ~ $2R_C$ ~11 nm) associated into more extended structures (size ~ $2R_g$ ~24 nm) and they demonstrate contacts at the distances comparably with their diameter ~ $2R_g$ that is visible as a weak peak at R~25-30 nm (Fig. 6b).

Conclusions

The used neutron techniques allowed confirming that the PIRAC treatment influences slightly the base properties of the bulk material. The results confirm the used neutron-based characterization techniques, additional to those employed hitherto (e.g., X-ray diffraction, scanning and transmission electron microscopy), to obtain additional key information on the considered material.

Acknowledgements

We acknowledge the support from CANAM (LM2015056) and LVR-15 (LM2015074) infrastructures. This work was also supported by a STSM Grant from COST Action CA16122.

References

Feigin, L.A., Svergun, D.I., 1987. Structure Analysis by Small-Angle X-Ray and Neutron Scattering. Plenum Press, New York, p. 335.

Mikula, P., Ryukhtin V., Rogante, M., 2019. On a possible use of neutron three axis diffractometer for studies of elastic and plastic deformation of polycrystalline materials. Submitted to Int. Conf. EAN 2019.

Rogante, M., Pasquini, U., Rosta, L., Lebedev, V., 2011a. Feasibility study for the investigation of Nitinol self-expanding stents by neutron techniques. Physica B: Condensed Matter 406, 527-532.

Rogante, M., Pasquini, U., Bonetti, M.G., 2011b. Applying Neutron Techniques to the Analysis of Nitinol Stents. European Medical Device Technology 2/9, 34-41.

Strunz, P., Saroun, J., Mikula, P., Lukas, P., Eichhorn, F., 1997. Double-Bent-Crystall Small-Angle Neutron Scattering Settings and Applications. J. Appl. Crystallogr. 30, 844-848.

Starosvetsky, D., Gotman, I. 2001. TiN coating improves the corrosion behavior of superelastic NiTi surgical alloy. Surface and Coatings Technology 148(2-3), 268-276.

Zorn, G., Adadi, R., Brener, R., Yakovlev, V.A., Gotman, I., Gutmanas, E.Y., Sukenik, C.N., 2008. Tailoring the Surface of NiTi Alloy Using PIRAC Nitriding Followed by Anodization and Phosphonate Monolayer Deposition. Chem. Mater. 20(16), 5368-5374.